Nonlocal Component of Radiative Flux Perturbation

Yi Ming[1] and V. Ramaswamy[1]

Yi Ming, Geophysical Fluid Dynamics Laboratory, Princeton, NJ 08542, USA. (Yi.Ming@noaa.gov)

V. Ramaswamy, Geophysical Fluid Dynamics Laboratory, Princeton, NJ 08542, USA.

[1]Geophysical Fluid Dynamics Laboratory,

Princeton, NJ

Abstract. Radiative flux perturbation (RFP) is defined as the top-of-the-atmosphere (TOA) radiative imbalance after the atmosphere-land system adjusts fully to an external perturbation, and serves as a useful metric for quantifying climate forcing. This paper presents an effort to address the issue whether a forcing imposed persistently over a specific region may alter the radiative balance elsewhere through atmospheric circulation, thus giving rise to a nonlocal component of RFP. We perturb the climate simulated with an atmospheric general circulation model (AGCM) solely by increasing the cloud droplet number concentration over the land, and observe widespread positive (warming) RFP over the ocean, along with the expected negative (cooling) RFP over the land. A detailed analysis suggests that the oceanic (or nonlocal) RFP is closely associated with a reduction in low cloud amount, which can be attributed primarily to the horizontal advection of drier land boundary layer air and to the oceanic boundary layer top entrainment of drier free troposphere air. By examining how the land surface and atmospheric energy balances are re-established, we are able to identify the physical mechanisms behind the strong hydrological impact of a tropical land shortwave (SW) forcing (the multiplier effect). In contrast, the hydrological cycle is relatively insensitive to an extratropical forcing.

1. Introduction

The instantaneous forcing (IF) and radiative flux perturbation (RFP) [*Hansen et al.*, 2005; *Haywood et al.*, 2009; *Lohmann et al.*, 2010] are two of the different definitions of radiative forcing. One can think of RFP as a superposition of IF and the ensuing top-of-the-atmosphere (TOA) radiative flux change from allowing the atmosphere and land to relax to a quasi-equilibrium state. For a regional forcing, IF is, by definition, confined locally. This may not be true for RFP as the impact of the forcing could propagate outside its boundary as part of the atmosphere-land adjustment. The nonlocal component of RFP can potentially alter the spatial pattern of the forcing, which plays an important role in determining the fully coupled regional climate response.

This issue is particularly relevant to anthropogenic aerosols, which are highly non-uniform owing to mostly land-based, localized emission sources and short (a few days) lifetimes. For example, one may ask whether the aerosols over the land can give rise to a RFP over the ocean. The answer has important implications for e.g., understanding their influence on the land-sea thermal contrast and monsoonal circulations. To our best knowledge, this topic has not been discussed widely in the literature, thereby posing an acute need for research.

In this paper, we devise a pair of atmospheric general circulation model (AGCM) experiments as a proof-of-concept of the nonlocal component of RFP. A detailed analysis focuses on the physical mechanisms crucial for explaining the findings.

2. Methodology

When judged by the skill in simulating the present-day climate, the Geophysical Fluid Dynamics Laboratory (GFDL) AM2.1 AGCM is one of the top-performing Intergovernmental Panel on Climate Change (IPCC) Fourth Assessment Report (AR4) models [*Reichler and Kim*, 2008]. A full description of the model formulation can be found in *The GFDL Global Atmospheric Model Development Team* [2004]. Only the physics parameterizations necessary for understanding the experimental design are recounted here.

AM2.1 uses the prognostic large-scale cloud scheme of *Tiedtke* [1993], with water vapor, cloud liquid and ice condensates and cloud amount being advected by model-generated winds. The cloud microphysics largely follows *Rotstayn* [1997] and *Rotstayn et al.* [2000]. The cloud droplet effective radius and autoconversion rate are linked explicitly to the droplet number concentration (N_d). In the default model configuration, N_d is set at 300 cm^{-3} over the land, 100 cm^{-3} over the ocean and linearly interpolated between two values at the land-ocean interface based on the measurements compiled by *Miles et al.* [2000]. These values reflect the fact that anthropogenic aerosols, which facilitate cloud formation by acting as cloud condensation nuclei, are usually more abundant over the land than over the ocean [*Boucher and Lohmann*, 1995]. Nonetheless, AM2.1 does not consider aerosol indirect effects [*Lohmann et al.*, 2010] as the specified N_d does not vary with aerosols explicitly.

A comparative case is constructed from lowering N_d over the land from 300 to 100 cm^{-3} while leaving N_d over the ocean unchanged (i.e., 100 cm^{-3} everywhere). Since N_d is expected to be lower in the absence of anthropogenic aerosols, the new setting may be somewhat closer to the pre-industrial condition. Both the default and comparative

experiments are forced with the observed climatological sea surface temperature (SST) and sea ice. Each is integrated from the same initial condition for 17 model years with the first year as spin-up (not analyzed).

3. Results

Since anthropogenic aerosols are located primarily over the Northern Hemisphere (NH) and their radiative effects are almost entirely in shortwave (SW), we choose to focus the analysis on the boreal summer months (June, July and August), during which the NH mean insolation is strongest. By definition, RFP arising from the increase in N_d over the land can be calculated as the difference in the TOA all-sky radiative flux (downward defined as positive) between the high and low N_d cases (the former minus the latter). In order to rigorously discern forced change from the model's natural variation, we compute the statistical significance of RFP using the Student's t-test, in which each model year is treated as an independent sample. We only show the results that are significant at the 95% confidence level (Fig. 1). Note that the same test is done for other variables as well.

The all-sky RFP features considerable radiative cooling over the land, except for the deserts and semi-arid areas (e.g., the Sahara and Arabian deserts, the interiors of Eurasia and the western United States) (Fig. 1(a)). The distinct spatial distribution results from the forcing being exerted through modifying clouds, which are far less prevalent over the dry regions. More intriguing is the widespread warming over the ocean, most notably in the subtropics and in the mid-latitudes (e.g., North Pacific and North Atlantic). This is an unambiguous evidence that a forcing posed solely over the land is capable of affecting remote oceanic areas. The task for us is to identify the physical mechanisms by which the oceanic (nonlocal) component of RFP is realized, and by doing so, to assess its robustness.

The clear- and cloudy-sky components of RFP are shown in Figs. 1(b) and 1(c), respectively. The former shows a small but extensive radiative warming, which is mostly in longwave (LW). As discussed later, this is due to the modestly lower land surface and atmospheric temperatures in response to the forcing. The close resemblance between the all- and cloudy-sky RFP, over the land and ocean alike, suggests that both the local and nonlocal components of RFP are tightly associated with cloud changes.

The differences in liquid water path (LWP) and low cloud amount (cloud top pressure greater than 680 hPa) – two key cloud properties – are shown in Figs. 2(a) and 2(b), respectively. LWP undergoes significant increases almost everywhere over the land (Fig. 2(a)). The largest ones coincides with the tropical rain belts (e.g., Central Africa, South and East Asia, Central America and the northern part of South America) and the mid-latitude storm tracks (e.g., the northernmost parts of Eurasia and North America). This can be explained by higher N_d inhibiting the autoconversion from cloud droplets to rain drops, and thus elevating the liquid condensate threshold for precipitation formation - a microphysical process that underlies the so-called second aerosol indirect (or "lifetime") effect [*Albrecht*, 1989]. Less straightforward is the modest but prevalent decrease in LWP over the ocean, often accompanied by reduced low cloud amount (Fig. 2(b)) with a correlation coefficient of 0.65. Because cloud amount and relative humidity (RH) are often linked in climate models as more moisture favors cloud formation [*Sherwood et al.*, 2010a], the decrease in low cloud amount can be thought of as a consequence of the widespread reduction in 850-hPa RH (Fig. 2(c)). The correlation coefficient between the changes in low cloud amount and RH is 0.70. Notable exceptions are the tropical Indian Ocean and two elongated areas over the southern Pacific Ocean, over which LWP increases. As

explained later, the former may be associated with an increase in oceanic precipitation as the thermal contrast between the Indian subcontinent and surrounding ocean weakens, while the latter is related to large-scale circulation changes. Another interesting feature is the significant reduction in RH (a few percents) over the aforementioned tropical land rain belts in spite of the substantially enhanced LWP. This does not occur over the mid-latitude land, where both RH and LWP increase.

Before any further investigation of atmospheric moisture content, it is warranted to examine the model's thermal response, which to some extent drives circulation (dynamical) changes. The differences in surface and 300-hPa temperatures are displayed in Figs. 3(a) and 3(b), respectively. A somewhat counterintuitive result is that despite the larger reduction in the SW incoming flux (Fig. 1(a)), the tropical land undergoes much smaller cooling than the extratropical land (Fig. 3(a)). Recalling that RH also varies differently between the tropics and extratropics, one may speculate that the two issues are probably intricately connected, and are best addressed in one theoretical framework (an attempt at which will be described in the discussion section). For the time being, let us take these results as given and see how they would help rationalize the simulated cloud changes.

The cooling at 300 hPa extends well beyond the land (Fig. 3(b)). The horizontal temperature gradient in the tropical upper troposphere is relatively weak due to the smallness of the local Coriolis parameter [*Sobel et al.*, 2001]. This mechanism accounts for the diffusive nature of the tropical cooling. The strong mid-latitude westerlies provide an effective means to homogenize the cooling within the zonal band. As a result, the meridional temperature gradient at ~30°N becomes stronger, giving rise to an acceleration of the local westerlies (not shown).

The variation in 850-hPa specific humidity (q) is rich in spatial structure (Fig. 4(a)). A good starting point for thinking about it is the governing equation of q. One can write the time rate of change of q as $-\mathbf{V} \cdot \nabla q - q\nabla \cdot \mathbf{V} + s$, where $\mathbf{V}$ is the wind vector and s is a sum of the source and sink terms. $-\mathbf{V} \cdot \nabla q$ represents the advection of moisture by winds, while $-q\nabla \cdot \mathbf{V}$ quantifies how the flow divergence affects q. Surface evaporation is the sole source of moisture in the boundary layer, and precipitation is the dominant sink term.

Two advection-related mechanisms, one in the horizontal direction and the other in the vertical direction, are central to understanding the tropical changes in q (Fig. 4(a)). First, as will be explained in the discussion section, there are negative anomalies over the tropical land rain belts (e.g., Central Africa and the northern part of South America). They are transported to the adjacent oceanic areas by near-equatorial easterlies (trade winds). Although this mechanism occurs mainly in the deep tropics, it cannot be used to explain the negative anomalies over Indonesia and the western Indian Ocean. Second, if one follows the Lagrangian-type argument that the RH of a local parcel is set remotely by the coldest temperature that the circulating parcel experienced [*Sherwood et al.*, 2010a, b], the colder upper troposphere (Fig. 3(b)) has an effect of dehydrating the subsiding air. The drier free troposphere air tends to lower the oceanic boundary layer RH and q through entrainment since the boundary layer temperature is tightly restricted by the fixed SST. This is responsible for the widespread reduction in the subtropical low cloud amount (Fig. 2(b)).

Advection also plays an important role in the mid-latitudes. The strong westerlies carry the negative (dry) anomalies in q over East Asia and the northeastern part of

North America over North Pacific and North Atlantic, respectively. Flow (circulation) change plays a lesser but appreciable role. The reduced land-sea thermal contrast (Fig. 3(a)) weakens the high pressure systems over North Pacific and North Atlantic through dynamical adjustment (Fig. 4(b)). The "warm advection" eastward of the anomalous lows gives rise to an increase in q, which translates into higher RH (Fig. 2(c)) as the lower tropospheric temperature is largely unchanged. Among the most notable examples of this mechanism are the elongated areas with increased q off the west coasts of North America and North Africa. Conversely, the "cold advection" westward of the anomalous lows tends to decrease q. The same effect gives rise to a pattern of alternating positive and negative anomalies in the Southern Hemisphere, which is present over the latitudinal band of $\sim$10°-45°S (Fig. 4(a)). From the viewpoint of macroturbulence [*Held*, 1999], one can perceive the circulation changes described here as a slowdown of the meridional heat and moisture exchanges (or mixing) facilitated by the oceanic high pressure systems (or anticyclonic eddies). This is consistent with the fact that the resulting moisture anomalies, positive and negative ones alike, are mostly in the meridional direction. In contrast, the advection by the mid-latitude westerlies occurs mainly in the zonal direction. Note that the above analysis focuses on the advection and flow divergence terms as precipitation does not vary much over these oceanic areas (not shown). This may be a consequence of the fixed SST, and is consistent with the argument that the spatial pattern of SST effectively controls the tropical rainfall distribution [*Neelin and Held*, 1987; *Lindzen et al.*, 1987].

4. Discussion

Once reaching quasi-equilibrium, a prescribed SST experiment has to operate under two energetic constraints, namely the land surface and atmospheric energy balances. The

former is more stringent as it has to be satisfied locally. The atmospheric energy balance holds only in the global-mean sense. With its temperature not varying with surface fluxes, the ocean acts as a heat reservoir.

The question crucial for understanding the model's atmosphere-land adjustment to a forcing is how the land surface regains energy balance after the initial radiative perturbation. In other words, how does the model climate manage to compensate for, in our case, a surface SW deficit? If one thinks about the energy exchanges between the different components of the climate system, this task can be accomplished in two steps. The first step calls for the land surface to lose less heat to the atmosphere. In the climatology, the SW absorption is balanced by the energy loss through LW, sensible heat (SH) and latent heat (LH) (Table 1). Conversely to the climatology, the model reacts to a SW deficit by simultaneously cutting all three terms to similar extents, as opposed to cutting LH alone [*Ramanathan et al.*, 2001]. This is true both for the tropics (30°S-30°N) and for the extratropics (elsewhere).

In the second step, the atmosphere over the land must find ways to make up for the decrease in land surface heating. Two options are available: emitting less LW radiation to space and/or drawing more energy from the rest of the atmosphere (and ultimately from the ocean). Interestingly, the extratropics are much more capable of altering the TOA outgoing LW radiative flux (OLR) than the tropics. The reduction in the extratropical land surface LW heating translates into virtually the same reduction in OLR, while the tropical OLR does not change much (Table 1). The reason for the different behaviors is two-fold. First, the inability of the tropical upper troposphere to sustain a strong temperature gradient (the weak temperature gradient approximation) means that SST

could play a dominant role in setting the upper tropospheric temperature, even over the land. Second, the relatively small land coverage in the tropics makes the role of SST even greater. Since SST is not allowed to vary, the tropical upper tropospheric temperature and OLR are strongly restricted. The situation in the extratropics is exactly the opposite, and thus favors weaker oceanic control over the extratropical land.

The above argument effectively leaves atmospheric adjustment as the only viable way to induce a net atmospheric heating over the tropical land. It manifests in the form of atmospheric energy convergence (AEC) averaged at 17.1 W m^{-2}, relative to the initial surface SW forcing of -9.0 W m^{-2} (Table 1). (Note that AEC is calculated as minus one times the sum of the diabatic terms.) The absolute value of their ratio (denoted as κ) can be viewed as a loosely defined measure of how effective the former is at compensating for the latter. κ is 1.9 for the perturbation, which is seemingly very different from the climatological value (0.3). This is largely due to the fact that as explained before, OLR, which plays a crucial role in venting the surface in the climatology, is no longer able to respond to a further perturbation to the land surface SW flux.

The hydrological cycle over the tropical land is an open system with a net exchange of moisture with the ocean. This is borne out in the fact that the climatological atmospheric latent heating (precipitation) is almost twice of the surface latent heat flux (evaporation) (Table 1). The transport (convergence) of oceanic moisture must make up the difference. For the perturbation, the reduced surface evaporation accounts for only 28% of the decrease in precipitation. A reduction in the moisture convergence (or a net divergence) is responsible for the rest. An important implication for understanding the hydrological impact of a SW forcing is that for the tropical land, every one watt per square meter

reduction in the net surface SW flux would lower the local rainfall by almost 0.05 mm day^{-1} (equivalent to 1.5 W m^{-2}) in what we call the *multiplier effect*. One can write precipitation (p) approximately as qM_c, where q is the boundary layer specific humidity and M_c is the convective mass flux out of the boundary layer [*Held and Soden*, 2006]. It follows that the fractional change in p ($\delta p/p$) is equal to $\delta q/q + \delta M_c/M_c$. The SW forcing reduces the tropical land precipitation substantially by 14% owing to the multiplier effect, while M_c decreases only by 6%. This explains why q is considerably lower over the tropical rain belts (Fig. 4(a)). The reduction in q also tends to lower RH as it outpaces the boundary layer temperature and associated saturated specific humidity changes.

In stark contrast, atmospheric adjustment presents an effective means (with a κ of 0.6) to offset the surface SW deficit over the extratropical land. The hydrological response is seriously damped, with a precipitation reduction of only 0.007 mm day^{-1} (equivalent to 0.2 W m^{-2}) for one watt per square meter of surface SW forcing. These attributes are due to two factors. First, about one third of the surface forcing is balanced by decreasing OLR, and thus does not involve precipitation change. Second, the hydrological cycle is closed over the extratropical land, meaning that most of the precipitation reduction will translate directly into lower surface evaporation. This proves to be another efficient way to compensate for the other two thirds of the surface SW forcing. It is interesting to note that using an AGCM with moist convective adjustment and diagnostic large-scale clouds, *Erlick et al.* [2006] found a similar latitudinal dependence of the climate response to an increase in SW cloud absorption.

We conclude by reiterating that strictly speaking, the above arguments apply only to the atmosphere-land (fast) response [*Andrews et al.*, 2010]. It is conceivable that the

fully coupled atmosphere-ocean (slow) response would be very different. For example, SST would decrease significantly as a result of the TOA radiative deficit (i.e., negative RFP). Nonetheless, the physical mechanisms discussed in this paper are useful not only for understanding the deviation of RFP, an increasingly used measure of radiative forcing, from the traditional instantaneous forcing, but also for elucidating the near-term (a few decades) climate change caused by anthropogenic aerosols as the ocean adjusts more slowly than the land due to thermal inertia. It is also worth noting that the response is caused by a change in cloud droplet number concentration – a purely scattering effect analogous to aerosol indirect effects. More work is needed to account for aerosol-induced atmospheric absorption in the general framework laid out here [*Ming et al.*, 2010].

References

Albrecht, B. A. (1989), Aerosols, cloud microphysics, and fractional cloudiness, *Science*, *245*, 1227–1230.

Andrews, T., P. M. Forster, O. Boucher, N. Bellouin, and A. Jones (2010), Precipitation, radiative forcing and global temperature change, *Geophys. Res. Lett.*, *37*, doi:10.1029/2010GL043991.

Boucher, O., and U. Lohmann (1995), The sulfate-CCN-cloud albedo effect: A sensitivity study using two general circulation models, *Tellus B*, *47*, 281–300.

Erlick, C., V. Ramaswamy, and L. M. Russell (2006), Differing regional responses to a perturbation in solar cloud absorption in the SKYHI general circulation model, *J. Geophys. Res.*, *111*, doi:10.1029/2005JD006491.

Hansen, J., et al. (2005), Efficacy of climate forcings, *J. Geophys. Res.*, *110*, doi: 10.1029/2005JD005776.

Haywood, J. M., L. J. Donner, A. Jones, and J.-C. Golaz (2009), Global indirect radiative forcing caused by aerosols: IPCC (2007) and beyond, in *Clouds in the Perturbed Climate System*, edited by J. Heintzenberg and R. Charlson, MIT Press, Cambridge, MA, USA.

Held, I. M. (1999), The macroturbulence of the troposphere, *Tellus A*, *51*, 59–70.

Held, I. M., and B. J. Soden (2006), Robust responses of the hydrological cycle to global warming, *J. Clim.*, *19*, 5686–5699.

Lindzen, R., B. Kirtman, D. Kirk-Davidoff, and E. K. Schneider (1987), On the role of sea surface temperature gradients in forcing low level winds and convergence in the tropics, *J. Atmos. Sci.*, *44*, 2418–2436.

Lohmann, L. R. U., T. Storelvmo, A. Jones, S. Menon, J. Quaas, A. Ekman, D. Koch, and R. Ruedy (2010), Total aerosol effect: radiative forcing or radiative flux perturbation?, *Atmos. Chem. Phys.*, *10*, 3235–3246.

Miles, N. L., J. Verlinde, and E. E. Clothiaux (2000), Cloud droplet size distributions in low-level stratiform clouds, *J. Atmos. Sci.*, *57*, 295–311.

Ming, Y., V. Ramaswamy, and G. Persad (2010), Two opposing effects of absorbing aerosols on global-mean precipitation, *Geophys. Res. Lett.*, *37*, doi:10.1029/2010GL042895.

Neelin, J. D., and I. M. Held (1987), Modeling tropical convergence based on the moist static energy budget, *Mon. Wea. Rev.*, *115*, 3–12.

Ramanathan, V., P. J. Crutzen, J. T. Kiehl, and D. Rosenfeld (2001), Aerosols, climate, and the hydrological cycle, *Science*, *294*, 2119–2124.

Reichler, T., and J. Kim (2008), How well do coupled models simulate today's climate?, *Bull. Amer. Meteor. Soc.*, *89*, 303–311.

Rotstayn, L. D. (1997), A physically based scheme for the treatment of stratiform clouds and precipitation in large-scale models. I: Description and evaluation of microphysical processes, *Quart. J. Roy. Meteor. Soc.*, *123*, 1227–1282.

Rotstayn, L. D., B. F. Ryan, and J. Katzfey (2000), A scheme for calculation of the liquid fraction in mixed-phase clouds in large-scale models, *Mon. Wea. Rev.*, *128*, 1070–1088.

Sherwood, S. C., W. Ingram, Y. Tsushima, M. Satoh, M. Roberts, P. L. Vidale, and P. A. O'Gorman (2010a), Relative humidity changes in a warmer climate, *J. Geophys. Res.*, *115*, doi:doi:10.1029/2009JD012585.

Sherwood, S. C., R. Roca, T. M. Weckwerth, and N. G. Andronova (2010b), Tropospheric water vapor, convection and climate, *Reviews of Geophysics*, *48*, doi:doi:10.1029/2009RG00030.

Sobel, A. H., J. Nilsson, and L. M. Polvani (2001), The weak temperature gradient approximation and balanced tropical moisture waves, *J. Atmos. Sci.*, *58*, 3650–3665.

The GFDL Global Atmospheric Model Development Team (2004), The new GFDL global atmosphere and land model AM2-LM2: Evaluation with prescribed SST simulations, *J. Clim.*, *17*, 4641–4673.

Tiedtke, M. (1993), Representation of clouds in large-scale models, *Mon. Wea. Rev.*, *121*, 3040–3061.

Figure 1. RFP (W m^{-2}) for all-sky (the upper panel), clear-sky (the middle panel) and cloudy-sky (the lower panel) conditions.

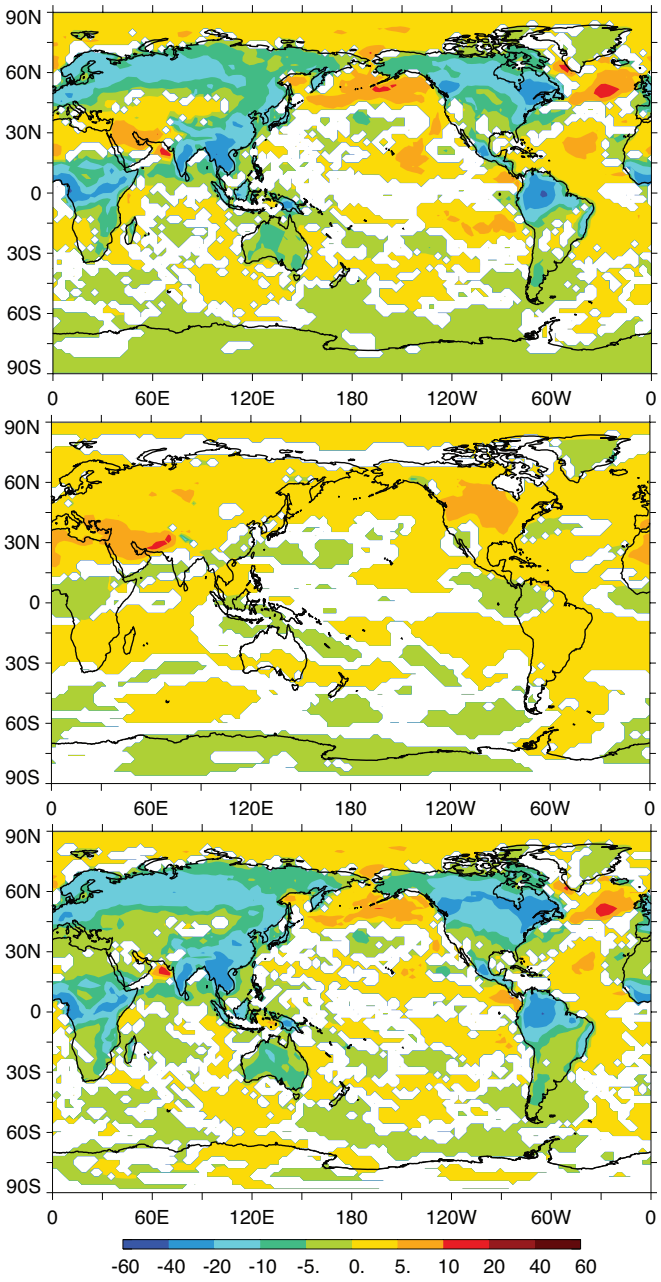

Figure 2. Changes in LWP (10^{-2} kg m^{-2}; the upper panel), low cloud amount (%; the middle panel) and 850-hPa RH (%; the lower panel) (colored shading). The climatological values are shown as contours.

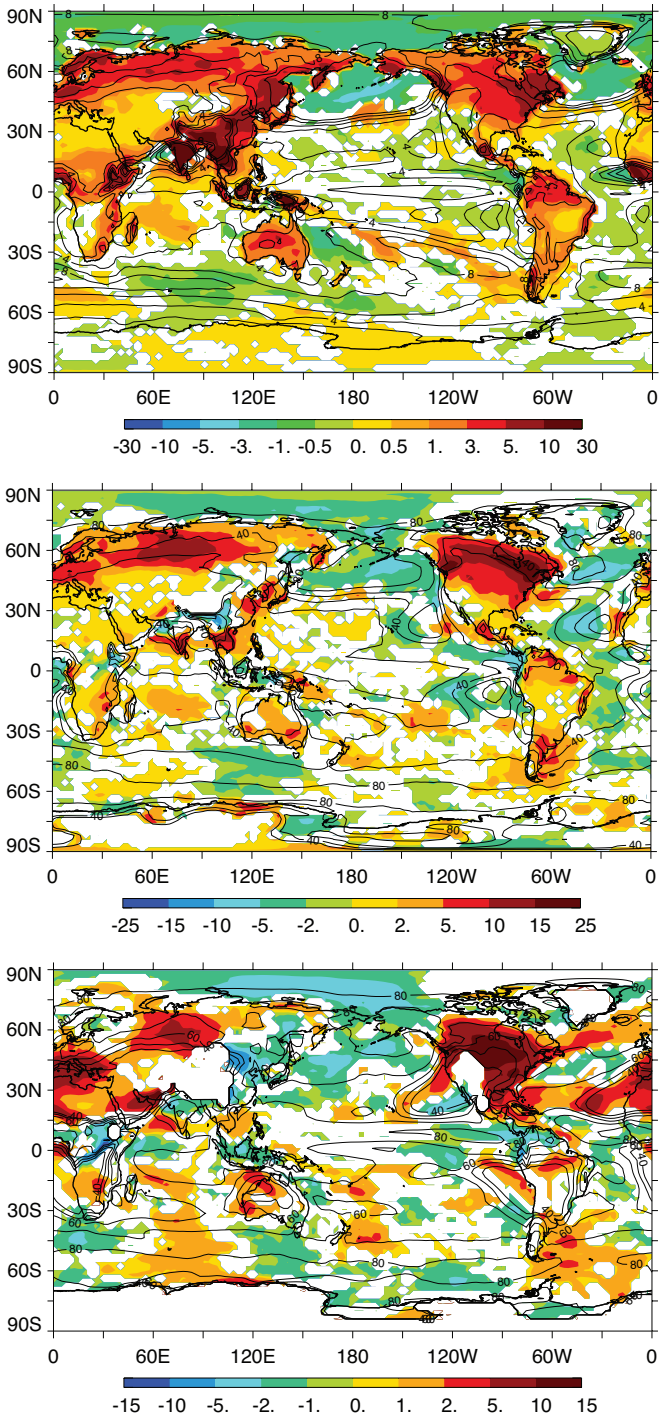

Figure 3. Changes in surface and 300-hPa temperatures (K; the upper and lower panels, respectively). The climatological values are shown as contours.

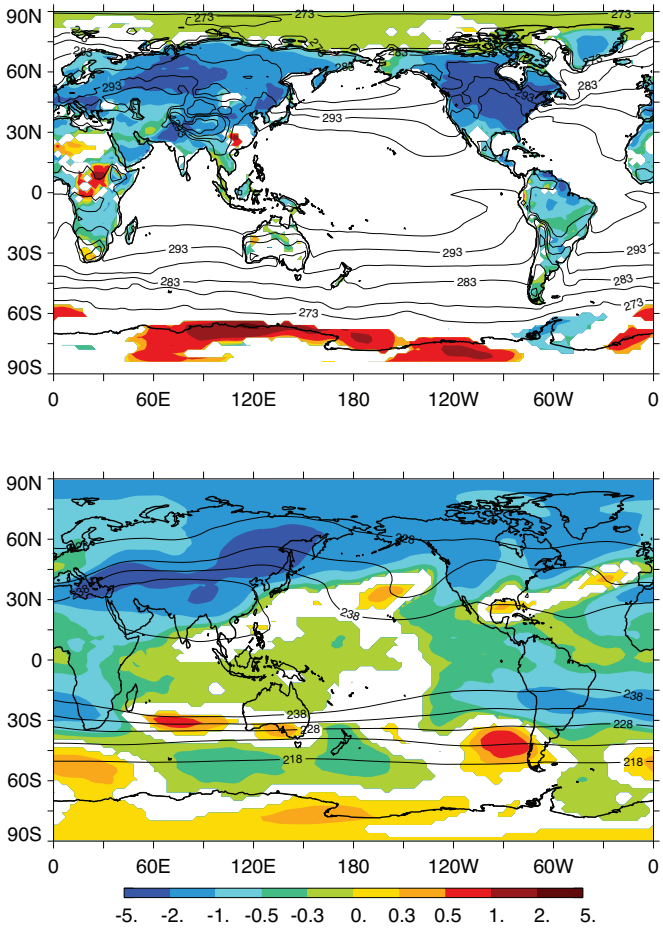

Figure 4. Changes in 850-hPa specific humidity (10^{-4} kg kg^{-1}; the upper panel) and SLP (hPa; the lower panel). The climatological values are shown as contours.

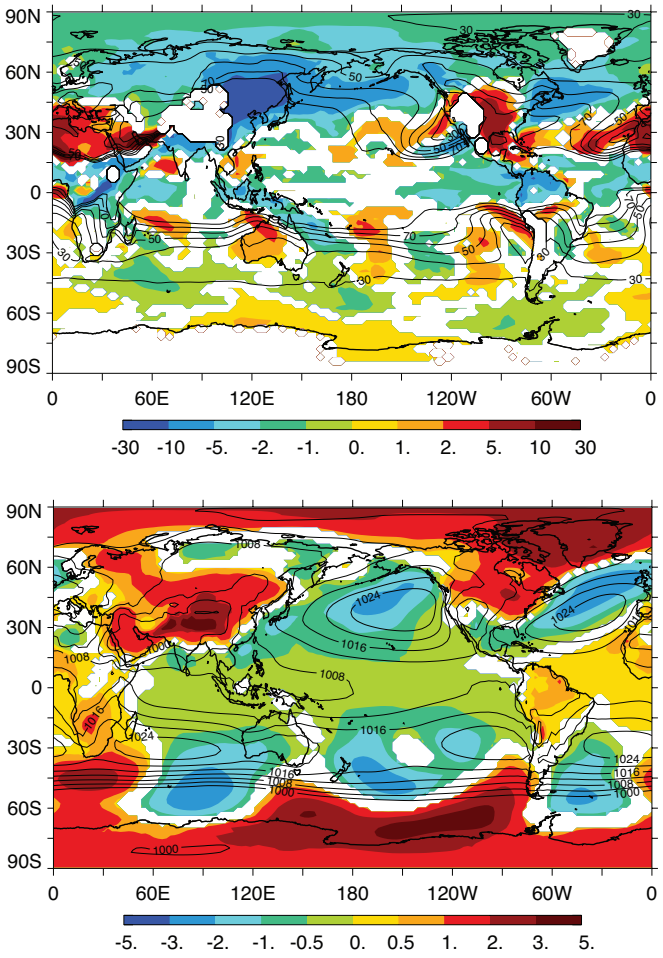

Table 1. Surface, TOA and atmospheric energy budgets over the tropical and extratropical land for the perturbation and climatology. The diabatic terms are shortwave (SW), longwave (LW), sensible heat (SH) and latent heat (LH). The atmospheric energy convergence (AEC) is calculated as minus one times the sum of the diabatic terms. The sign convention is downward as positive for the surface and TOA, and heating as positive for the atmosphere. All numbers are area-weighted. The unit is W m^{-2}.

	Surface				TOA		Atmosphere				
	SW	LW	SH	LH	SW	LW	SW	LW	SH	LH	AEC
Pert. (Tropics)	-9.0	2.3	2.2	3.8	-7.7	-0.3	1.3	-2.6	-2.2	-13.6	17.1
Clim. (Tropics)	187.6	-77.9	-51.6	-54.8	283.9	-263.3	96.3	-185.4	51.6	97.2	-59.7
Pert. (Extratropics)	-9.7	3.3	3.7	1.5	-9.2	3.2	0.5	-0.1	-3.7	-2.1	5.4
Clim. (Extratropics)	161.3	-68.9	-37.4	-42.1	242.7	-233.7	81.4	-164.8	37.4	50.0	-4.0